α-Mangostin Inhibits LPS-Induced Bone Resorption by Restricting Osteoclastogenesis Via NF-κB and MAPK Signaling

Wenkan Zhang
Zhejiang University School of Medicine
guangyao Jiang
Zhejiang University School of Medicine
xiaozhong zhou
Zhejiang University School of Medicine
leyi huang
Zhejiang University School of Medicine
jiahong meng
Zhejiang University School of Medicine
bin he
Zhejiang University School of Medicine
yiying qi (qiyiying@zju.edu.cn)
Zhejiang University School of Medicine

Research Article

Keywords: osteoclast, α-mangostin, NF-κB, MAPK, osteolysis.

Posted Date: December 13th, 2021

DOI: https://doi.org/10.21203/rs.3.rs-1141803/v1

Abstract

Background: Excessive activation of osteoclasts is an important cause of imbalance in bone remodeling, which further leads to pathological bone destruction. This is a clear feature of many osteolytic diseases, such as rheumatoid arthritis, osteoporosis, and osteolysis around the prosthesis. Based on the fact that many natural compounds have therapeutic potential for treating these diseases by suppressing osteoclast formation and function, we proved that α-mangostin, a natural compound isolated from mango, might be a promising choice. α-mangostin was described had anti-inflammatory, anticancer and cardioprotective effects.

Methods: We evaluated the therapeutic effect of α-mangostin in the process of osteoclast formation and bone resorption. The receptor activator of NF-κB ligand (RANKL) induces the formation of osteoclasts in vitro, and the potential pathways of α-mangostin to inhibit the differentiation and function of osteoclasts were explored. A mouse model of LPS-induced calvarial osteolysis was establish. Subsequently, micro-CT, histology, etc. were used to evaluate the effect of α-mangostin in preventing inflammatory osteolysis.

Results: In our study, we found that α-mangostin could inhibit RANKL-induced osteoclastogenesis and reduced osteoclast-related gene expression *in vitro*. Besides, F-actin ring immunofluorescence and resorption pit assay indicated that α-mangostin can also destroy the function of osteoclast. Furthermore, α-mangostin achieved these effects by disrupting the activation of NF-κB/MAPKs signaling pathways. *In vivo*, our data revealed that α-mangostin could protect mouse calvarial from osteolysis.

Conclusions: Together, our study demonstrates that α-mangostin exhibit the ability of inhibiting steoclastogenesis both *in vitro* and *in vivo*, and may be a potential option for treating osteoclast-related diseases.

Introduction

Bone remodeling is regulated by the balance between osteoclastic bone resorption and osteoblastic bone formation, which is an important metabolic process that regulates bone structure and function[1]. Current research showed that, originating from hematopoietic monocyte/macrophage precursors is the only known cell that has the function of resorbing bone in human body[2,3]. Excess osteoclast activity leads to excessive osteoclastic bone resorption, disrupts the balance between bone resorption and bone formation, and causes a variety of bone disorders, including osteoporosis, rheumatoid arthritis, periodontal disease and metastatic cancers[4,5]. Therefore, inhibiting the activity of osteoclasts might be the available strategy for such diseases.

Receptor activators of nuclear factor-κB (NF-κB) ligand (RANKL) and macrophage colony-stimulating factor (MCSF) have been shown to mediate osteoclast differentiation by activating different signaling cascades, such as nuclear Factor-κB (NF-κB) and mitogen-activated protein kinase (MAPK) signaling pathway[6–8]. These signaling pathways will promote the expression of transcription factors including AP-

1 and NFATc1, which are the key transcription factors for osteoclast differentiation, and finally enhance the differentiation and activation of monocyte-macrophage precursors into osteoclasts[9,10]. Wherefore drugs that suppress RANKL-induced signaling pathways have great potential to prevent these diseases. In our study, the effect of α-mangostin (later written as mangostin) on RANKL-induced NF-κB activation and osteoclastogenesis was explored.

Mangostin, the most representative xanthone isolated from the pericarp of mangosteen, was reported to have a variety of pharmacological effects[11]. Specifically, mangostin has potential usage in anticancer and can be regarded as a chemoprevention or agent for oral cancer, colon cancer, pancreatic cancer, breast cancer and cutaneum carcinoma, etc[12,13]. In addition, its anti-inflammatory, anti-bacterial, anti-malarial, anti-obesity action was reported before[11,14–16]. Furthermore, mangostin has the effects of maintaining cardiovascular and digestive system health, as well as controlling free radical oxidation[17–19]. Recent researchers have shown that mangostin can inhibit osteoarthritis (OA) progress by suppressing the mitochondrial apoptosis of chondrocytes that induced via an activation of the NF-kB pathway[20]. Nevertheless, the researches of the effects of mangostin on osteoclasts and osteolytic diseases are not comprehensive enough[21]. Based on the results previously revealed that mangostin had potential therapeutic value in the treatment of OA through inhibiting the production of NO and PGE2 and the IL-1β induced phosphorylation of the NF-kB signaling pathway, we hypothesized that mangostin might be a novel candidate for treatment of osteoclast-related diseases by inhibiting osteoclastogenesis.

In our current research, we first studied the effects of mangostin on the formation and function of RANKL-induced osteoclastogenesis, then explored its mechanism and discovered two key signaling pathways, NF-kB and MAPK signaling. Finally, the bone protection effect of mangostin was verified in the mouse LPS osteolysis calvarial model.

Materials And Methods

Media and reagents

α-mangostin (CAT:M3824, purity >98%, Figure 1A) was purchased from Sigma-Aldrich (St. Louis, MO, United States). Dulbecco's modified Eagle's medium (DMEM), Alpha modification of Eagle's medium (α-MEM), fetal bovine serum (FBS), and penicillin/streptomycin were purchased from Gibco-BRL (Gaithersburg, MD, United States). Recombinant mouse macrophage colony-stimulating factor (M-CSF) and RANKL were acquired from R&D Systems (Minneapolis, MN, United States). The specific primary antibodies that obtained from Cell Signaling Technology (Danvers, MA, United States) are as follows: c-Fos (#2250), nuclear factor of activated T cells c1 (NFATc1) (#8032), and β-tubulin (#2146), phospho-JNK (#4668), IκBα (#4814), phospho-IκBα (#2859), p65 (#8242), phospho-p65 (#3033), phospho-IKKα/β (#2697), IκB kinase β (IKKβ) (#8943), ERK (#4695), phospho-ERK (#4370), JNK 1/2 (#9252), p38 (#9212), phospho-p38 (#4511), TRAP(#92345), Human-reactive STING pathway antibody sampler

kit(#38866). CTSK (ab37259) were obtained from Abcam. TRAP staining kit, berberine and anisomycin were purchased from Sigma-Aldrich unless otherwise noted.

TABLE 1 Primers used for quantitative PCR

Gene	Forward (F) and reverse (R) primer sequence (5′–3′)
GAPDH	F: ACCCAGAAGACTGTGGATGG
	R: CACATTGGGGGTAGGAACAC
CTSK	F: CTTCCAATACGTGCAGCAGA
	R: TCTTCAGGGCTTTCTCGTTC
TRAP	F: CTGGAGTGCACGATGCCAGCGACA
	R: TCCGTGCTCGGCGATGGACCAGA
DC-STAMP	F: AAAACCCTTGGGCTGTTCTT
	R: AATCATGGACGACTCCTTGG
c-Fos	F: CCAGTCAAGAGCATCAGCAA
	R: AAGTAGTGCAGCCCGGAGTA
NFATc1	F: CCGTTGCTTCCAGAAAATAACA
	R: TGTGGGATGTGAACTCGGAA
CTR	F: TGGTTGAGGTTGTGCCCA
	R: CTCGTGGGTTTGCCTCATC

In vitro bone marrow-derived macrophage isolation and osteoclast differentiation

Bone marrow cells were acquired from the long bones of 6-week-old male C57BL/6 mice, as described previously[22], and the bone marrow cells in femurs and tibias were flushed out and cultured in α-MEM supplemented with 10% FBS, 100 U/ml penicillin, 100 μg/ml streptomycin and 25 ng/ml M-CSF at 37°C for 5 days to differentiate into bone marrow-derived macrophages (BMMs). Next, cells were respectively seeded into a 48-well plate approximately 1×10^4 cells per well in triplicate and were treated with various concentrations of mangostin (0, 0.5, 1, 2, or 4 μmol/L) in the presence of 25 ng/mL M-CSF and 50 ng/ml RANKL. Culture medium was replaced every two days. After culturing for 5 days, the cells were fixed with

4% paraformaldehyde (PFA) and then stained for TRAP based on the instructions. TRAP-positive multinucleated cells (nuclei number, ≥3) were counted using a light microscope (BX51; Olympus).

Cell Viability Assay

To test the effects of mangostin on BMMs viabilities, a CCK8 Kit was performed. Based on the manufacturer's instruction, cells were seeded in a 96-well plate (8×10^3 cells per well) and cultured in complete α-MEM medium for 48 h or 96 h in the different concentrations of mangostin (0–4 μM). Next, CCK8 reagent (10 ul) was added to each well, and the plate was incubated for another 2-4 h. The optical density (OD) was measured using a MR7000 microplate reader (Dynatech, NV, USA) at 450 nm. The viabilities of BMMs exposed to mangostin were expressed as a percentage of untreated cells.

Constructing stable overexpression cell lines (transfection)

An ACP5 gene overexpression plasmid and negative control (NC) plasmid were purchased from Genepharma Corporation (Shanghai, China). All the procedures were followed with the manufacture protocols. The transfected cells were treated with 2 μg/mL puromycin until all the cells died in the control group (untransfected cells). Before used for further analysis, the transfection efficiency of the cells was further confirmed by western blot.

Hoechst 33342 staining

4×10^5 cells per well were planted into a six-well plate and treated with different concentrations of mangostin for 5days, culture changed every 2 days, then cells were cultured with Hoechst 33342 for 20 mins. Finally, a fluorescence microscope (Olympus, Tokyo, Japan) was utilized to visualize morphological changes of apoptotic cells at 365 nm.

Apoptosis Flow Cytometry Assay

Apoptosis was measured using the reagent Annexin V-FITC/PI apoptosis kit (Multi-Sciences, Hangzhou, Zhejiang, China). 2×105 per well BMMs were planted in a 6-well plate and cultured with different concentrations of mangostin (0, 0.5, 1, 2 μmol/L) for 24 hrs. After washed with PBS and collected, the cells were incubated with Annexin V-FITC/PI apoptosis kit for 20 min in the dark. All steps are based on the manufacturer's protocols. V-FITC (+)/PI (−) and Annexin V- FITC (+)/PI (+) staining signified cells that were in the early and later stages of apoptosis, respectively. All the samples were quantized and analyzed by a flow cytometer (FACSCalibur, BD, San Jose, CA, USA).

In vitro Osteoclast Differentiation

BMMs were planted into a 96-well plate at a density of 8×10^3 cells per well, and cultured in complete α-MEM supplemented with 25 ng·ml×1 M-CSF, 50 ng·ml×1 RANKL, and different concentrations of mangostin (0, 0.5, 1, and 2 μM). Culture medium was replaced every 2 days. 5 days later, after washed twice with PBS, cells were fixed with 4% paraformaldehyde (PFA), and stained for TRAP. TRAP-positive cells (nuclei number, ≥3) were counted as mature osteoclasts under a light microscope.

RNA Extraction and Quantitative PCR Assay

Total RNA from cultured cells was extracted using the Trizol reagent (Invitrogen, Carlsbad, CA, USA) guided by the manufacturer's protocols. Complementary DNA (cDNA) was synthesized from 1 μg of total RNA using PrimeScript RT Master Mix (TaKaRa Biotechnology, Otsu, Japan). Real-time PCR was performed using the TB Green Premix Ex Taq kit (TaKaRa Biotechnology) on a StepOnePlus Real-Time PCR System (Applied Biosystems, Foster City, CA, USA). Each reaction was run at the following conditions: 95°C for 60 s and then 40 cycles of 95°C for 10 s, 60°C for 20 s and 72°C for 20 s. GAPDH was regarded as endogenous controls. The mouse primer sequences are shown in Table 1.

F-Actin Ring Immunofluorescence and Resorption Pit Assay

In order to visualize F-actin rings, BMMs were treated with 25ng/ml M-CSF and 50ng/ml RANKL for 4 days. 2 × 103 cells/cm2 number of differentiated osteoclasts were seeded onto bovine bone slices and allowed to adhere overnight. Then cells were treated with different concentrations of mangostin (0, 0.5, 1, and 2 μM) for another 2 days. Next, cells were fixed with 4% PFA for 15 min, and permeabilized with 0.4% Triton X-100 for 10 min, then stained with rhodamine-conjugated phalloidin (1:200; Invitrogen Life Technologies, Carlsbad, CA, United States) diluted in 0.5% bovine serum albumin (BSA)–PBS for 30min. Fluorescent images were captured utilizing a fluorescence microscope (EU5888, Leica, Wetzlar, Germany) and analyzed by ImageJ software (National Institutes of Health, Bethesda, MD, United States). Then, in order to observe resorption pits, these bone slices were washed twice with PBS, and cells that had adhered to the bone slices were removed by mechanical brushing. Bone slice images were acquired with a scanning electron microscope (SEM; S-4800, Hitachi, Japan) and analyzed by ImageJ software.

Western Blotting

The main signaling pathways affected by mangostin were detected by western blotting. Cells were treated with or without 2 μM mangostin for 4 h, then were stimulated with 50 ng·mL×1 RANKL for 0, 5, 10, 20, 30, or 60 min. To explore the effects of mangosin on c-Fos and NFATc1 expression, BMMs were seeded in a 6-well plate (1×10^5 cells per well) and cultured with 25 ng·mL∗1 M-CSF and 50 ng·mL×1 RANKL in the presence or absence of 2 μM mangostin for 0, 2, 4, or 6 days. After being collected, the cells were lysed with RIPA buffer (Sigma-Aldrich, St. Louis, MO, USA), which included protease inhibitor and phosphatase inhibitor cocktail (Sigma-Aldrich). According to the steps in the manufacturer's protocols, the supernatant was collected. A BCA protein assay kit (Beyotime) was used to quantify the total amount of protein. The equal amounts of protein samples were separated by 8–15% SDS-PAGE at 75 V for 1.5 h and subsequently transferred onto 2.2 um polyvinylidene fluoride membranes (Millipore, Billerica, MA, USA) at 250 mA for 2 h in a humid atmosphere. The membranes were blocked with 10% milk or 5% bovine serum albumin (BSA; Sigma-Aldrich) and incubated with the primary antibody overnight at 4°C. After being washed with TBST for three times, 10 min each time, the membranes were incubated with horseradish peroxidase (HRP)-conjugated secondary antibodies (Huabio, Hangzhou, Zhejiang, China) for 1 h at room temperature. The target bands were observed and development using an enhanced chemiluminescence kit (Millipore).

Mouse model of LPS-induced calvarial osteolysis

All animal care and experimental protocols were designed and performed in compliance with National Institutes of Health (NIH) guide for the care and use of Laboratory Animals and the Guide of the Animal Care Committee of Zhejiang University. Thirty 6-week-old male C57BL/6 mice weighing 18-22 g were purchased from Experimental Animal Center of Zhejiang University. A mouse model of LPS-induced calvarial osteolysis was established, as described previously, to explore the effects of mangostin on inflammatory bone loss *in vivo*. After acclimatizing to the laboratory for 1 week, mice were randomly divided into the following three experimental groups (n = 5 per group): sham, LPS (vehicle) and LPS + mangostin groups. After anesthetized with intraperitoneal sodium pentobarbital (50 mg·kg−1), the cranial periosteum of mice was separated, and 5 mg/kg body weight LPS (Sigma-Aldrich) in PBS were embedded under the periosteum at the middle suture of the calvaria in the LPS (vehicle) and LPS + mangostin groups on days 1 and 4, while PBS was injected in the sham group. Then, the mice in the LPS + mangostin group were subcutaneous administered 10 mg/kg mangostin every day for 7 days. Mice in the sham and LPS groups were administered PBS intragastrically as a control. mangostin doses were determined according to previous studies.17, 26 on day 7, all the mice were sacrificed and their calvarial were harvested for subsequent analysis.

Micro-CT scanning

The calvaria were measured (n = 5 per group) by a high-resolution micro-CT (Skyscan 1072, Aartselaar, Belgium). The scanning protocol was set at an isometric resolution of 9 μm and X-ray energy settings of 80 kV and 80 μA. Then, a three-dimensional (3D) reconstruction was performed, and a square area of interest (ROI, 3 mm × 3 mm) surrounding the midline suture was selected for further qualitative and quantitative analysis. Bone volume/tissue volume (BV/TV), number of porosities, and percentage of porosity for each specimen were measured as reported previously (Wedemeyer et al., 2007).

H&E and TRAP Staining of Tissue Sections

Fixed samples (n = 5 per group) were decalcified in 10% EDTA (pH = 7.4) for 2 weeks, and then embedded in paraffin. Next, the Calvaria were cut into 4-μm-thick histological sections for further hematoxylin and eosin (H&E) and TRAP staining. The sections were detected and photographed under a light microscope (TE2000-S; Nikon, Tokyo, Japan). Histomorphometry parameters of BV/TV, erosion area, the number of TRAP-positive osteoclasts, and surface area of osteoclasts per bone surface (OcS/BS) were assessed for each sample.

Statistical Analysis

All data are expressed as mean ± standard deviation (SD). Each experiment was repeated at least three times separately and the results were analyzed with Prism 6.01 (GraphPad Software, La Jolla, CA, United States). A two-tailed, unpaired Student's t-test was used for the comparisons between two groups. One-way ANOVA with post hoc Newman-Keuls test was used to analyze differences in multiple comparisons. Values of $P < 0.05$ were considered statistically significantly different.

Results

Preventive effect of mangostin on RANKL-Induced Osteoclast differentiation in vitro

To evaluate potential cytotoxic effect of mangostin on bone marrow-derived macrophages (BMMs), a cell viability assay was performed. BMM cells were treated with different concentrations of mangostin (0, 0.5, 1, 2, 4umol/L) for 48 or 96 h. The results of CCK-8 revealed that mangostin caused no obvious cytotoxicity on BMM cells at concentrations not higher than 2μmol/L (figure 1B). Apoptosis Flow Cytometry Assay shows that mangotin at a concentration of 0-2 umol/L does not cause apoptosis of BMMs, and the absence of significant changes in apoptosis-related proteins also confirms this (figure 2). When the concentration of mangostin reached 4μM, the flow cytometry results indicated 64.94% of apoptotic BMMs. In addition, Hoechst33342, as a classic method of observing apoptotic cell nucleus shrinkage, also showed that there was cell apoptosis under the 4μM mangostin. The corresponding changes in the expression of apoptotic proteins also confirmed this phenomenon (figure S1). According to this, we choose 2μmol/L as the highest concentration in subsequent experiments.

In order to explore the preventive effect of mangostin on osteoclastogenesis, BMM cells were treated with different concentrations of mangostin (0, 0.5, 1, 2μmol/L) in the presence of M-CSF (25 ng/mL) and RANKL (50 ng/mL). After 5 days of incubation, the osteoclasts of differentiation of BMM cells by TRAP stain. As shown in figure 1C and D, mangostin reduces osteoclast differentiation in a dose-dependent manner. There were a lot of mature TRAP-positive multinucleated osteoclasts in the control group, while in the mangostin group, the number and area of osteoclasts were significantly decreased. In addition, the results showed that the higher the dose of mangostin, the better the effect of inhibiting osteoclast differentiation. Next, mangostin was added at different stages of osteoclast formation to further study that on which stage of osteoclast formation that mangostin has an inhibitory effect. Specifically, cells were treated with 2 μM mangostin at early stage (day 1-2), middle stage (day 3–4), late stage (day 5–6) and whole stage (day 1-6). In figure 1E and F, compared with the other groups, the number and size of osteoclasts were significantly reduced in the whole stage and early-stage groups. Correspondingly, there was a slight decrease in the middle-stage group and this inhibition effect was not significant in the late-stage mangostin group. Finally, we explored whether the inhibitory effect of mangostin would be offset when BMMs overexpress the TRAP gene (ACP5). We constructed stable transfected cells overexpressing ACP5 (S2A), and again evaluated the number and size of osteoclast. Despite the presence of mangostin, osteoclasts overexpressing ACP5 can regain the physiological function of bone resorption. This result confirmed that TRAP was a key node for mangostin to hinder osteoclastogenesis. After overexpression of ACP5, despite the inhibitory effect of mangostin, BMMs could still be induced to differentiate into osteoclasts, but the size and number were reduced compared to the control group (figure S1D4). All in all, these data indicated that mangostin had a suppressive effect on osteoclast formation, especially at the early stage of osteoclast differentiation.

Mangostin decreases the RANKL-stimulated osteoclast-specific gene expression

Next, we further investigated the effect of mangostin on RANKL-stimulated osteoclast-specific gene expression. After pretreated with mangostin at concentrations of 0, 0.5, 1, or 2 μmol/L for 4 hour, BMM cells were stimulated by RANKL (50 ng/mL) for 48 hours. The results of RT-PCR further proved that mangostin suppressed the expression levels of osteoclasts-related genes, which included cathepsin K (Ctsk), Dc-stamp, TRAP, CTR, V-ATPase-d2 and NFATc1 in time-dependent (figure 3A) and dose-dependent manner (figure 3B). These data meant that mangostin showed a preventive effect on osteoclastogenesis.

Preventive effect of mangostin on bone resorption in vitro

Previously, the role of mangostin in inhibiting osteoclast formation had been revealed, so we wondered if it could extenuate the function of osteoclasts. BMM cells (1×10^4 cells/well) were seeded on Osteo Assay Plate and then incubated with RANKL and M-CSF with different concentrations of mangostin for 5-6 days. The tight F-actin ring is an essential condition for osteoclasts to perform bone resorption. SO, we can observe it to evaluate whether mature osteoclasts are functioning. From the results of immunofluorescence, we conclude that the shape and size of the F-actin ring can be destroyed by mangostin, and statistics show that the degree of such abuse is dose-dependent (figure 4A). As shown in figure 4B and C, extensively bone resorption area and larger size per pit were observed in the control group, while treatment of mangostin decreased the pit area significantly, and almost no resorption pits were found on the bone slices treated with 2 μM mangostin. Similarly, we also verified the effect of overexpression of ACP5 on mangostin's inhibition of osteoclast function. Despite the presence of mangostin, osteoclasts overexpressing ACP5 can regain the physiological function of bone resorption (figure S2B3). Together, our results indicate that mangostin suppresses the F-actin ring formation and bone resorptive activity of mature osteoclasts *in vitro*.

Mangostin inhibits RANKL-Induced NF-κB and MAPK Signaling Pathways

First, we verified at the protein level that mangostin can inhibit the expression of osteoclast-related proteins induced by RANKL in a dose-dependent manner (figure 5A and B). Compared with the group stimulated by RANKL alone, the experimental group pretreated with mangostin inhibited the expression of NFATc1, c-Fos, CTSK, and TRAP, especially within 3-5 days after adding RANKL.

NF-κB signalling is regarded as a key role in osteoclast differentiation, we wondered whether the effect of mangostin on RANKL-stimulated osteoclastogenesis via regulation of NF-κB activation or not[5]. In this study, the phosphorylation and protein levels of NF-κB p65 and IκBα were measured by Wstern blot assay. Before stimulated with 50ng/mL RANKL for 1 hour, the BMMs were preincubated with different concentration of mangostin for 4 hours. In figure 5C and D, cells treated with mangostin showed less expression of phosphorylation level of NF-κB p65 and IκBα, and degradation of IκBα was also significantly decreased. In addition, MAPK (ERK, JNK, and p38) were phosphorylated by the stimulation of RANKL, while mangostin treatment could significantly suppressed the phosphorylation levels of the above proteins (figure5E). In figure 5F, the results of the quantitative analysis confirmed our conclusions.

We used the JNK agonist anisomycin to carry out the flip experiment. The results suggested that mangostin indeed inhibited the activation of the JNK pathway, but the ability of mangostin that hindered the formation and function of osteoclasts was not eliminated (figure S1D5 and S2B4, C). These results revealed that mangostin inhibits RANKL-induced activation of NF-κB and MAPK signalling *in vitro*.

Effect of mangostin on LPS-induced Osteolysis in a Mouse Calvarial Model

To investigate effects of mangostin on pathological osteolysis *in vivo*, an LPS-induced murine calvarial osteolysis model was established. LPS were embedded under the periosteum at the middle suture of the calvaria with or without mangostin (10mg/kg) in LPS (vehicle) and LPS + mangostin groups. Mice in the LPS + mangostin group were intragastrically administered 10 mg/kg mangostin every day for 7 days. Mice in the sham and LPS (vehicle) groups were administered PBS intragastrically as a control. After 7 days, the calvaria were collected and fixed in 4% paraformaldehyde solution, then analyzed by microcomputed tomography (CT) and histology (Figure 6A). Micro-CT images showed the bone loss of calvaria was decreased by mangostin treatment, while extensive bone erosion on the calvaria were observed in LPS (vehicle) groups compared with the sham group. Quantitative analysis indicated that decline of BV/TV and ascension of porosity induced by LPS were all retarded by mangostin treatment (Figure 6B).

Additionally, histological assessment further confirmed the results from Micro-CT that mangostin had the therapeutic effect on osteolysis. In figure 6C, hematoxylin and eosin (H&E) staining showed that LPS induced severe osteolytic changes in the LPS (vehicle) group, and significant reduced extent of bone erosion were found in the mangostin group. What's more, the number of osteoclasts was decreased in mangostin group compared with LPS (vehicle) group via TRAP staining (figure 6E). These data suggested that mangostin hindered LPS-induced osteolytic bone loss *in vivo*.

Discussion

Increased osteoclast-induced bone resorption is an important factor leading to periprosthetic osteolysis and osteoporosis[2,23]. As the balance between osteoblast-mediated bone formation and osteoclast-mediated bone resorption have been reported to be responsible for bone turnover and remodeling, it is important to find out an available strategy on them for the treatment of these diseases[5]. In our study, we figured out for the first time that mangostin could inhibit RANKL-induced osteoclastogenesis through inhibition of NF-κB and MAPK signaling *in vitro* and hinders LPS-induced osteolytic bone loss in a mouse calvarial model.

Mangostin has been investigated possessing extensive biological activities and pharmacological properties–antioxidant, antineoplastic, anti-proliferation and induces apoptosis[14,24,25]. Recent report reveals the use of mangostin in treating rheumatoid arthritis and a mangostin-loaded self-micro emulsion (MG-SME) was designed[25]. Recently, it has been reported that mangostin can block LPS-induced

activation in RAW264.7 cells, thereby inhibiting the secretion of IL-1β, IL-6, NO and COX-2[26]. Mangostin had been reported via inhibiting the activation of TAK1-NF-κB to exert anti-inflammatory effects, which makes it a potential choice for treating inflammatory diseases[27]. Previous studies have shown that mangostin has an inhibitory effect on the osteoclast differentiation of RAW264.7 cells. However, compared with RAW264.7 cells, it is more scientific to select mouse bone marrow-derived macrophages as the research object for in vitro experiments, and the results produced are more credible, which can also explain the effects in vivo. What's more, we confirmed the role of mangostin in inhibiting osteoclasts at the animal level. Our current research reminds us that mangostin has great potential for treating osteoporosis.

At the beginning, we wandered if mangostin had a toxic effect on BMMs and whether it can inhibit the osteoclast differentiation. The results of CCK-8 reminded us that mangostin had no obvious inhibitory effect on BMMs cells at concentrations lower than 2μmol/L. In order to determine that the effect of mangostin on the formation of osteoclasts is indeed achieved by inhibiting their differentiation rather than promoting cell apoptosis, we also did apoptosis flow cytometry assay and western blotting, and the results were consistent with our previous conclusions. In supplementary figure 1, we clearly found that when the mangostin dose reached 4μM, the expression of apoptosis-related protein was significantly increased. The flow cytometry results suggested that there was apoptosis in BMM cells, and the results of Hoechst staining further confirmed this conclusion. This is the basis for our follow-up study to select the drug dosage. TRAP staining showed that at concentrations below cytotoxic levels, mangostin treatment had a significant protective effect on RANKL-induced osteoclast differentiation. As the concentration of mangostin increased, the number of TRAP-positive cells decreased, and mature osteoclasts were scarcely observed in the high-concentration (2 μmol/L) treatment group. Based on the conclusions of previous studies of natural compounds, the inhibitory effect of berberine on osteoclast formation was used as our positive control[28]. To further study at which stage of osteoclastogenesis mangostin unleashed its inhibitory effect, we added mangostin (2 μmol/L) at different stages of osteoclastogenesis. The experimental results were in line with our expectations. As shown in figure 1D, the earlier the mangostin intervention, the stronger the effect of obstructing osteoclast formation. Compared with the control group, the osteoclastogenesis inhibition of mangostin was hardly seen in the late-stage group. Based on the above data, we concluded that mangostin could inhibit the formation of osteoclasts, especially in the early stage of osteoclastogenesis.

Under the stimulation of RANKL, the up-regulation of the expression of several specific genes is closely related to the differentiation of osteoclasts[8]. Therefore, real-time PCR was then utilized to measure the inhibitory effect of mangostin on RANKL-induced mRNA expression of these genes (TRAP, NFATc1, CTSK, V-ATPase d2, CTR and DC-stamp). As expected, results indicated that mangostin blocked RANKL-stimulated osteoclast-related genes in a dose and time-dependent. This proved from another aspect that mangostin indeed suppressed the osteoclasts differentiation. After verifying the inhibitory effect of mangostin on osteoclast formation and RANKL-induced osteoclastic marker gene expression, it was naturally explored whether mangostin can also function in osteoclast bone resorption. The results that

large bone resorption in the control group and less number and area of bone resorption in the mangostin group demonstrated the hinder effect of mangostin on osteoclast function.

NF-κB signalling is a very classic pathway in those studies of osteoclastogenesis[7]. When RANKL activates downstream signals, the phosphorylation of NF-κBp65 and IκBα and the degradation of IκBα promote the activation of NF-κB p65 and nuclear translocation, which will increase the expression of s osteoclast-specific gene and promote the formation and function of osteoclasts[29,30]. Based on this status quo, many researchers currently focus their research on pharmacological intervention for NF-κB signalling related checkpoints. In our current study, we found that mangostin restricted the degradation of IκBα and phosphorylation of NF-κB p65 and IκBα induced by RANKL stimulation. Furthermore, many previous studies have shown that RANKL-induced osteoclastogenesis usually involves the activation of both NF-κB and MAPK signaling pathways. So, in this study, we explored whether mangostin could also inhibit the activation of the MAPK pathway. Not surprisingly, the phosphorylation of all three MAPK pathways (ERK, JNK, and p38) in BMMs stimulated with RANKL was blocked by mangostin at non-cytotoxicity concentrations.

Previous studies reported that JNK1 regulates RANKL-induced osteoclastogenesis by activating the Bcl-2-Beclin1-autophagy pathway, and our findings suggest that the JNK pathway is regulated by mangostin[31]. So, we chose anisomycin, a JNK activator, to explore whether the mangostin-mediated inhibition of osteoclastogenesis can be reversed. The results confirmed that anisomycin could indeed reverse the effect of mangostin on the JNK pathway, but the effect of mangostin on inhibiting the formation and function of osteoclasts will not be affected. This may be due to the fact that mangostin works through the three MAPK pathways, so simply changing one of them does not make a significant difference. When the LPS pathway is activated, the TRAF-TBK1-IRF3 pathway will also change[32]. We used western blot assay to detect the expression of TBK1 and IRF3 proteins, and found that the presence of mangostin did not affect the pathway stimulation of RANKL. Therefore, we concluded that the activation of MAPK and NF-KB pathways was inhibited by mangostin, except for IRF3 (figure S2D).

Since previous results indicated that mangostin obstructed RANKL-induced osteoclast formation and decreased the expression of those osteoclastic related gene via blocking the NF-κB and MAPK signaling cascades *in vitro*, we investigated whether mangostin could inhibit pathological osteolysis in an LPS-induced murine calvarial osteolysis model[33]. Analysis of Micro-CT scan results and histological examinations, we concluded that mangostin did have the effect of reducing LPS-induced osteolysis *in vivo*. Regarding the choice of *in vivo* drug dosage and administration method, we refer to the method of previous literature[34,35]. At first, we chose 20mg/kg as the *in vivo* dose, and we found that there was inflammatory hyperplasia under the skin of the mouse skull. So, we choose to reduce the body dose to 10mg/kg, which is consistent with the effective dose of another research[36]. In our study, we reported for the first time that mangostin could be used as a potential treatment for these osteoclast-related diseases.

Nevertheless, there are several limitations of the current study. First, since this balance consists of osteoclastic bone resorption and osteoblastic bone formation, further research on the effect of

mangostin on osteoblasts are needed to be addressed. Then, the present study proved that mangostin markly suppressed the RANKL-induced osteoclast formation by inhibiting the pathway *in vitro*. We still need to study whether mangostin also exerts its anti-osteoclastogenesis effect through this pathway *in vivo*. Unfortunately, we did not explore the exact binding target of mangostin. This target should explain why the presence of mangostin affects the blockade of NF-κB and MAPK pathways caused by RANKL. In the early stage of the RANKL pathway, after RANKL binds to RANK, tumor necrosis factor receptor-related factor 6 (TRAF6) will be recruited to form a complex, and then further activate the MAPK and NF-κB pathways[37,38]. Since the MAPK and NF-κB pathways share the same upstream promoter TRAF6, it is reasonable to speculate that M plays an interfering role in the binding process of TRAF6 and RANK.

Conclusion

In summary, in this study, we showed that mangostin inhibited RANKL-induced osteoclastogenesis and bone resorption *in vitro*. And these inhibitory effects were mediated by suppressing the RANKL-induced NF-κB and MAPK signal pathways. In addition, mangostin had demonstrated its protective effect on LPS-induced inflammatory bone loss *in vivo*, indicating that it can be used as a potential drug to prevent or treat osteoclast-related diseases.

Abbreviations

α-MEM: Alpha modification of Eagle's medium; BMM: bone marrow-derived macrophages; CTSK: cathepsin K; DMEM: Dulbecco's modifed Eagle's medium; DMSO: Dimethylsulfoxide; FACS: Fluorescence Activating Cell Sorter; FITC: Fluorescein Isothiocyanate; HE: Hematoxylin–eosin; HRP: Horseradish Peroxidase; IHC: Immunohistochemistry; MAPK: Mitogenactivated protein kinase; M-CSF : macrophage colony-stimulating factor ; NC: negative control; NF-κB : nuclear factor-κB ;OA: osteoarthritis ;PBS: Phosphate buffered saline; PI: Propidium Iodide; RANKL :Receptor activators of NF-κB ligand SD: Standard Deviation; TRAF 6: tumor necrosis factor receptor-related factor 6 ;TRAP: tartrate resistant acid phosphatase;

Declarations

Funding

This work was supported by grants from the National Natural Science Foundation of China (No. 81772325 and No. 82072413).

Acknowledgements

Gratitude should be expressed to the colleagues of Key Laboratory of Motor System Disease Research and Precision Therapy of Zhejiang Province, clinical research center and animal laboratory of the Second

Affiliated Hospital Zhejiang University School of Medicine for giving precious help in this research.

Author contributions

All authors contributed to data analysis, drafting or revising the article, gave final approval of the version to be published, and agree to be accountable for all aspects of the work.

Data sharing statement

The data used to support the findings of this study are available from the corresponding author upon request.

Ethics approval and consent to participate

All experiments were carried out in accordance with the guidelines of the

Ethics Committee of Zhejiang University and approved by the Research Ethics

Committee of the Second Afliated Hospital of Zhejiang University School of

Medicine, China

Consent for publication

Not applicable.

Competing interests

The authors declare that they have no competing interests.

References

1. Kylmaoja E, Nakamura M, Tuukkanen J. Osteoclasts and Remodeling Based Bone Formation. Current stem cell research & therapy 2016;11:626–33.
2. Boyle WJ, Simonet WS, Lacey DL. Osteoclast differentiation and activation. Nature 2003;423:337–42.
3. Soysa NS, Alles N. Osteoclast function and bone-resorbing activity: An overview. Biochemical and biophysical research communications 2016;476:115–20.
4. Raynaud-Messina B, Verollet C, Maridonneau-Parini I. The osteoclast, a target cell for microorganisms. Bone 2019;127:315–23.
5. Ono T, Nakashima T. Recent advances in osteoclast biology. Histochemistry and cell biology 2018;149:325–41.
6. Nagy V, Penninger JM. The RANKL-RANK Story. Gerontology 2015;61:534–42.

7. Boyce BF, Xing L. Biology of RANK, RANKL, and osteoprotegerin. Arthritis research & therapy 2007;9 Suppl 1:S1.
8. Feng W, Guo J, Li M. RANKL-independent modulation of osteoclastogenesis. Journal of oral biosciences 2019;61:16–21.
9. Boyce BF, Xing L. Functions of RANKL/RANK/OPG in bone modeling and remodeling. Archives of biochemistry and biophysics 2008;473:139–46.
10. Walsh MC, Choi Y. Biology of the RANKL-RANK-OPG System in Immunity, Bone, and Beyond. Frontiers in immunology 2014;5:511.
11. Chen G, Li Y, Wang W, Deng L. Bioactivity and pharmacological properties of alpha-mangostin from the mangosteen fruit: a review. Expert opinion on therapeutic patents 2018;28:415–27.
12. Markowicz J, Uram L, Sobich J, Mangiardi L, Maj P, Rode W. Antitumor and anti-nematode activities of alpha-mangostin. European journal of pharmacology 2019;863:172678.
13. Zhang KJ, Gu QL, Yang K, Ming XJ, Wang JX. Anticarcinogenic Effects of α-Mangostin: A Review. Planta medica 2017;83:188–202.
14. Wang F, Ma H, Liu Z, Huang W, Xu X, Zhang X. alpha-Mangostin inhibits DMBA/TPA-induced skin cancer through inhibiting inflammation and promoting autophagy and apoptosis by regulating PI3K/Akt/mTOR signaling pathway in mice. Biomedicine & pharmacotherapy = Biomedecine & pharmacotherapie 2017;92:672–80.
15. Wang MH, Zhang KJ, Gu QL, Bi XL, Wang JX. Pharmacology of mangostins and their derivatives: A comprehensive review. Chinese journal of natural medicines 2017;15:81–93.
16. Ge Y, Xu X, Liang Q, Xu Y, Huang M. alpha-Mangostin suppresses NLRP3 inflammasome activation via promoting autophagy in LPS-stimulated murine macrophages and protects against CLP-induced sepsis in mice. Inflammation research: official journal of the European Histamine Research Society [et al] 2019;68:471–9.
17. Gupta SC, Kunnumakkara AB, Aggarwal S, Aggarwal BB. Inflammation, a Double-Edge Sword for Cancer and Other Age-Related Diseases. Frontiers in immunology 2018;9:2160.
18. Taher M, Mohamed Amiroudine MZ, Tengku Zakaria TM, Susanti D. α-Mangostin Improves Glucose Uptake and Inhibits Adipocytes Differentiation in 3T3-L1 Cells via PPARγ, GLUT4, and Leptin Expressions. 2015;2015:740238.
19. Kosem N, Ichikawa K, Utsumi H, Moongkarndi P. In vivo toxicity and antitumor activity of mangosteen extract. Journal of natural medicines 2013;67:255–63.
20. Pan T, Chen R, Wu D, et al. Alpha-Mangostin suppresses interleukin-1β-induced apoptosis in rat chondrocytes by inhibiting the NF-κB signaling pathway and delays the progression of osteoarthritis in a rat model. International immunopharmacology 2017;52:156–62.
21. Li Y-H, Hong R-H, Liang Y-M, Pan H-S, Cheng Z-H. Alpha-mangostin suppresses receptor activator nuclear factor-κB ligand-induced osteoclast formation and bone resorption in RAW264.7 cells by inhibiting the extracellular signal-regulated kinase and c-Jun N-terminal kinase signaling. Pharmacognosy Magazine 2018;14:390.

22. Wang W, Wu C, Tian B, et al. The inhibition of RANKL-induced osteoclastogenesis through the suppression of p38 signaling pathway by naringenin and attenuation of titanium-particle-induced osteolysis. International journal of molecular sciences 2014;15:21913–34.
23. Kenkre JS, Bassett J. The bone remodelling cycle. 2018;55:308–27.
24. Sheng X, Li J, Zhang C, et al. alpha-Mangostin promotes apoptosis of human rheumatoid arthritis fibroblast-like synoviocytes by reactive oxygen species-dependent activation of ERK1/2 mitogen-activated protein kinase. Journal of cellular biochemistry 2019;120:14986–94.
25. Pan-In P, Wongsomboon A, Kokpol C, Chaichanawongsaroj N, Wanichwecharungruang S. Depositing α-mangostin nanoparticles to sebaceous gland area for acne treatment. Journal of pharmacological sciences 2015;129:226–32.
26. Franceschelli S, Pesce M, Ferrone A, et al. A Novel Biological Role of α-Mangostin in Modulating Inflammatory Response Through the Activation of SIRT-1 Signaling Pathway. Journal of cellular physiology 2016;231:2439–51.
27. Zou W, Yin P, Shi Y, et al. A Novel Biological Role of alpha-Mangostin via TAK1-NF-kappaB Pathway against Inflammatory. Inflammation 2019;42:103–12.
28. Han SY, Kim YK. Berberine Suppresses RANKL-Induced Osteoclast Differentiation by Inhibiting c-Fos and NFATc1 Expression. The American journal of Chinese medicine 2019;47:439–55.
29. Lawrence T. The nuclear factor NF-kappaB pathway in inflammation. Cold Spring Harbor perspectives in biology 2009;1:a001651.
30. Hoesel B, Schmid JA. The complexity of NF-κB signaling in inflammation and cancer. Molecular cancer 2013;12:86.
31. Ke D, Ji L, Wang Y, et al. JNK1 regulates RANKL-induced osteoclastogenesis via activation of a novel Bcl-2-Beclin1-autophagy pathway. FASEB journal: official publication of the Federation of American Societies for Experimental Biology 2019;33:11082–95.
32. Fehervari Z. Meta-inflammation and IRF3. Nature immunology 2016;17:1015.
33. Komori T. Animal models for osteoporosis. European journal of pharmacology 2015;759:287–94.
34. Willson CM, Grundmann O. In vitro assays in natural products research - a matter of concentration and relevance to in vivo administration using resveratrol, α-mangostin/γ-mangostin and xanthohumol as examples. Natural product research 2017;31:492–506.
35. Yin Q, Wu YJ, Pan S, et al. Activation of Cholinergic Anti-Inflammatory Pathway in Peripheral Immune Cells Involved in Therapeutic Actions of α-Mangostin on Collagen-Induced Arthritis in Rats. Drug design, development and therapy 2020;14:1983-93.
36. Pan T, Wu D, Cai N, et al. Alpha-Mangostin protects rat articular chondrocytes against IL-1β-induced inflammation and slows the progression of osteoarthritis in a rat model. International immunopharmacology 2017;52:34–43.
37. Honma M, Ikebuchi Y, Suzuki H. RANKL as a key figure in bridging between the bone and immune system: Its physiological functions and potential as a pharmacological target. Pharmacology &

therapeutics 2021;218:107682.
38. Wada T, Nakashima T, Hiroshi N, Penninger JM. RANKL-RANK signaling in osteoclastogenesis and bone disease. Trends in molecular medicine 2006;12:17–25.

Figures

Figure 1

Mangostin inhibits RANKL-induced osteoclastogenesis in vitro. (A), The molecular structure of mangostin comes from the official website of sigma-aldrich. (B), BMMs were treated with different concentrations of mangostin for 48h or 96 h, and viability of BMMs was measured by CCK-8 assay. (C), BMMs were treated with M-CSF (25 ng/ mL) and RANKL (50 ng/mL) in the presence pf the indicated mangostin concentrations for 5 days. Cells were then stained for TRAP activity and were photographed. (D), The number and area of TRAP-positive cells were analyzed. (E), BMMs were stimulated with M-CSF and RANKL for 5 days, and 2 μmol/L mangostin was added at different stages. Scale bars:200 μm (upper layer of C, E),500 μm (Lower layer of C, E). (F), The number and area of TRAP-positive cells were analyzed. Data are presented as mean ± SD. ∗∗P < 0.01, ∗∗*P < 0.001, compared with the controls

Figure 2

Mangostin does not induce the apoptosis of BMMs in vitro. (A), BMMs were treated with different concentrations of mangostin for 5 days, and the level of apoptosis was measured by flow cytometry. (B), The expression of those apoptosis-related proteins, which including BCL-2 and BCL-XL, was measured by a Western blot assay. Error bar = mean ± SD.

Figure 3

Mangostin suppresses RANKL-induced expression of osteoclast-related genes. (A), BMMs were treated with M-CSF, RANKL and different concentrations of mangostin for 5 days. (B), BMMs were cultured with M-CSF (25 ng/ mL) and RANKL (50 ng/mL), with or without 2 μmol/L mangostin, for 0, 1, 3 or 5 days. The mRNA expression of those osteoclast-related genes, including TRAP, CTSK, CTR, V-ATPase d2, NFATc1, DC-STAMP, was determined by qPCR. Data are shown as mean ± SD. ∗P < 0.05, ∗∗P < 0.01, ∗∗*P < 0.001, compared with the controls.

Figure 4

Mangostin attenuates bone resorptive activity of mature osteoclasts and inhibits F-actin ring formation in vitro. Same number of BMM-derived mature osteoclasts were seeded onto bovine bone slices and were treated with the indicated mangostin concentrations for 2 days. (A), The cells were stained with rhodamine-conjugated phalloidin and representative fluorescence microscope images of F-actin rings.are shown. scale bar = 20 μm. (B), Representative images of bone resorption pits were acquired by scanning electron microscopy (SEM); scale bar = 100 μm. (C), The resorption area of bone discs and the size of F-actin rings were quantified using the ImageJ software. Error bar = mean ± SD. ∗∗P < 0.01, ∗∗∗P < 0.001, compared with the controls.

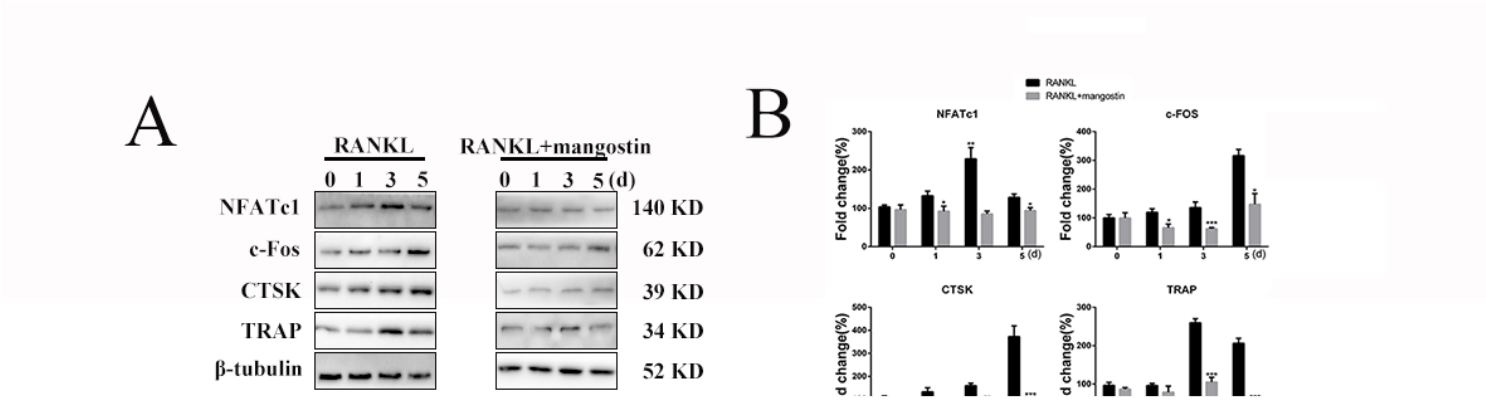

Figure 5

Mangostin inhibits osteoclastogenesis by specifically suppressing RANKL-induced phosphorylation of NF-κB/MAPK signaling pathways. (A)The protein expression levels of NFATc1 c-FosTRAP and CTSK in BMMs treated with 50 ng/mL RANKL with or without 2 μM mangostin for 0, 1, 3, or 5 days. (C, E), BMMs were pretreated with or without 2 μM mangostin for 4 h and then cultured with RANKL for the indicated periods. (D, F) The gray levels of phosphorylated p65, ERK, JNK, and p38 were quantified and normalized relative to their total protein counterparts. The gray levels of p-IκBα and IκBα were normalized to β-tubulin. Data are presented as mean ± SD. ∗P < 0.05, ∗∗P < 0.01, ∗∗∗P < 0.001, compared with RANKL alone.

Figure 6

Mangostin prevents LPS-induced bone loss inhibiting osteoclast activity in a mouse calvarial model. (A), Representative micro-CT reconstruction images of the calvarial each group. Scale bars = 1 mm. (B), Quantitative analysis of the bone volume against tissue volume (BV/TV, %) and the percentage of porosity (%) was performed using the micro-CT data. (C), Representative images of H&E staining of calvarial bone sections from sham, vehicle, and 2 μM mangostin-treated groups. Scale bars = 200 μm. (D), Histomorphometric analysis of the BV/TV and erosion area was performed. (E), Representative images of TRAP staining of calvarial bone sections from three groups; cale bar = 50 μm. (F), Quantitative analysis of the number of TRAP-positive osteoclasts, and the percentage of osteoclast surface per bone surface (OcS/BS, %) were performed. * P < 0.05 and **P < 0.01, ∗∗∗P < 0.001, compared with the mice in the vehicle group.

Supplementary Files

This is a list of supplementary files associated with this preprint. Click to download.

- S1.tif